Pluripotent stem cell-derived bile canaliculi-forming hepatocytes to study genetic liver diseases involving hepatocyte polarity

Overeem, Arend W; Klappe, Karin; Parisi, Silvia; Klöters-Planchy, Petra; Mataković, Lavinija; du Teil Espina, Marines; Drouin, Christian A; Weiss, Karl Heinz; van IJzendoorn, Sven C D

Published in:
Journal of Hepatology

DOI:
10.1016/j.jhep.2019.03.031

Document Version
Final author's version (accepted by publisher, after peer review)

Publication date:
2019

Accepted Manuscript

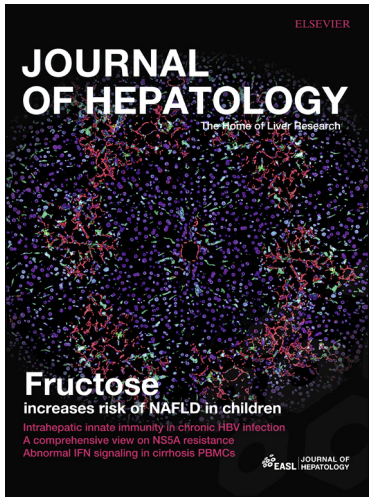

Pluripotent stem cell-derived bile canaliculi-forming hepatocytes to study genetic liver diseases involving hepatocyte polarity

Arend W. Overeem, Karin Klappe, Silvia Parisi, Petra Klöters-Planchy, Lavinija Mataković, Marines du Teil Espina, Christian A. Drouin, Karl Heinz Weiss, Sven C.D. van IJzendoorn

PII: S0168-8278(19)30225-9
DOI: https://doi.org/10.1016/j.jhep.2019.03.031
Reference: JHEPAT 7319

To appear in: *Journal of Hepatology*

Received Date: 30 July 2018
Revised Date: 15 March 2019
Accepted Date: 31 March 2019

Please cite this article as: Overeem, A.W., Klappe, K., Parisi, S., Klöters-Planchy, P., Mataković, L., du Teil Espina, M., Drouin, C.A., Weiss, K.H., van IJzendoorn, S.C.D., Pluripotent stem cell-derived bile canaliculi-forming hepatocytes to study genetic liver diseases involving hepatocyte polarity, *Journal of Hepatology* (2019), doi: https://doi.org/10.1016/j.jhep.2019.03.031

Pluripotent stem cell-derived bile canaliculi-forming hepatocytes to study genetic liver diseases involving hepatocyte polarity

Arend W. Overeem[1], Karin Klappe[1], Silvia Parisi[2], Petra Klöters-Planchy[3], Lavinija Mataković[1], Marines du Teil Espina[1], Christian A. Drouin[4], Karl Heinz Weiss[3], Sven C. D. van IJzendoorn[1*]

[1]*Department of Biomedical Sciences of Cells and Systems, University of Groningen, University Medical Center Groningen, Groningen, The Netherlands,* [2]*Department of Molecular Medicine and Medical Biotechnology, University of Naples Federico II, Naples, Italy,* [3]*University Hospital Heidelberg, Internal Medicine IV, Heidelberg, Germany,* [4]Service de Dermatologie, Centre Hospitalier du Grand Portage, Rivière du Loup, Québec, Canada

[*]Correspondence: prof. dr. Sven C.D. van IJzendoorn, Department of Biomedical Sciences of Cells and Systems, University Medical Center Groningen, Antonius Deusinglaan 1, 9713 AV, Groningen, the Netherlands. Telephone: (+31) (0)50 3616209 or +31 (0)50 3616111 (secretariat); E-mail: s.c.d.van.ijzendoorn@umcg.nl

Conflict of interests: none

Financial support: This work was in part funded by a 'Gastrostart' grant from the Dutch Gastroenterology Foundation (Nederlandse Vereniging voor Gastroenterology).

Author contributions: AO, KK, SP, LM, PK and ME: experiments and procedures. AO and SIJ: study design. AO, SIJ, CD and KW: data interpretation and writing of manuscript.

Keywords: Wilson disease; hepatocyte polarity, pluripotent stem cells, disease model

Abstract

Background & Aims: Hepatocyte polarity is essential for the development of bile canaliculi and transport of bile and waste products such as copper safely out of the liver. Genetically inherited defects in polarized processes can cause severe diseases. Functional studies of autologous mutated proteins in the context of the polarized hepatocyte have been challenging because of the lack of appropriate cell models. The aim of this study was to obtain a patient–specific hepatocyte model that recapitulated hepatocyte polarity and to employ this model to study endogenous mutant proteins in liver diseases that involve hepatocyte polarity. **Methods:** Patients' and control subjects' urine cell-derived pluripotent stem cells were differentiated towards hepatocyte-like cells. **Results:** Polarized hepatocyte-like cells (hiHeps) that formed *in vivo*-like bile canaliculi could be generated from embryonic and patient urine cell-derived pluripotent stem cells. HiHeps recapitulated polarized protein trafficking processes, exemplified by the Cu^{2+}-induced redistribution of the copper transporter protein ATP7B to the bile canalicular domain. We demonstrated that, in contrast to the current dogma, the most frequent yet enigmatic Wilson disease-causing ATP7B-H1069Q mutation *per se* did not preclude trafficking of ATP7B to the *trans*-Golgi Network. Instead, it prevented its Cu^{2+}-induced polarized redistribution to the bile canalicular domain, unrepairable by pharmacological folding chaperones. Finally, we demonstrate that hiHeps from a MEDNIK disease patient suffering from liver copper overload of unclear etiology showed no defect in the Cu^{2+}-induced redistribution of ATP7B to the bile canaliculi. **Conclusions:** Functional cell polarity can be achieved in patient pluripotent stem cell-derived hepatocyte like cells, and allow for the first time the study of the endogenous mutant proteins, patient-specific

pathogenesis and drug responses for diseases where hepatocyte polarity is a key aspect.

Lay summary

This study demonstrates that cells that are isolated from urine can be reprogrammed in a dish towards hepatocytes that display architectural characteristics similar as seen the intact liver. The application of this methodology to cells from patients diagnosed with inherited copper metabolism-related liver diseases (that is, Wilson disease and MEDNIK syndrome) revealed unexpected and novel insights into patient mutation-specific disease mechanisms and drug responses.

Introduction

Hepatocytes are polarized cells, exemplified by the segregation of their plasma membranes into basolateral/sinusoidal and apical/canalicular domains [1,2]. Hepatocyte polarity is essential for many hepatocyte-specific functions [1]. Not surprisingly therefore, loss of hepatocyte polarity is correlated with liver diseases [2]. In inherited liver diseases, mutations in specific genes can cause a defect in the targeting, expression and/ or function of proteins that display a steady state residence at either sinusoidal or canalicular surface domain [2].

Some proteins adopt a polarized distribution in hepatocytes only under specific circumstances. For example, the copper transporter protein ATP7B normally resides in the trans-Golgi Network (TGN) but when intracellular copper levels become too high ATP7B displays a polarized translocation to the bile canalicular domain where excess copper is excreted [3,4]. Mutations in the *ATP7B* gene in patients with Wilson disease (WD) [5] lead to excess copper deposition and damage to the liver and brain [6]. Some mutations have been reported to impair the intracellular trafficking of the mutant ATP7B protein [7,8]. However, for several, including the frequent H1069Q mutation in the Caucasian WD population [9], their impact on the polarized trafficking of the mutant ATP7B to the bile canalicular domain in response to excess copper is unknown. Similarly, the impact of mutations in the traffic regulatory gene *AP1S1* on the trafficking of ATP7B in hepatocytes of patients with MEDNIK syndrome, a disease with parallels to WD [10] has been postulated but not experimentally addressed.

Patients' biopsies provide information about the steady-state distribution of mutant proteins, but not about the regulated dynamics of mutant proteins such as the polarized trafficking of ATP7B mutants in copper-exposed cells. Studies of mutant

proteins including WD ATP7B mutants required their heterologous overexpression [11–14] in cancer cell lines, a strategy with several drawbacks [15]. Therefore, there is an urgent need for a cell culture system that recapitulates the trafficking of endogenously expressed mutant proteins in polarized human hepatocytes. Patient-own cells are the ideal source to study endogenous mutant proteins. The ability to generate induced pluripotent stem cells (iPSC) from patients' cells and to differentiate these to hepatocytes has been a major step towards the study of endogenous mutant proteins, including ATP7B, in physiologically relevant cell types [16–24]. However, the potential of iPSC-derived hepatocytes to polarize and form bile canaliculi, and their potential to study the polarized trafficking of endogenously expressed mutant protein, is not known.

Here, we characterized the potential of human pluripotent stem cell-derived hepatocytes to develop apical-basal polarity, bile canaliculi, and recapitulate polarized trafficking processes. We investigated their potential to study the functionalities of endogenous mutant proteins in human diseases where hepatocyte polarity is a key aspect, in this case the copper-stimulated redistribution of (mutant) ATP7B to the bile canalicular domain. This study reveals unexpected results with implications for proposed disease mechanisms and novel therapeutic strategies.

Materials and methods

Generation of induced pluripotent stem cells

WD iPSC cells from the homozygous patient were generated as described previously [25]. WD iPSC cells from the heterozygous patient were generated from urine-derived cells [26]. Informed consent was obtained from all subjects. Briefly, at 75% confluence, urine-derived cells were transduced with the lentiviral vector pRRL.PPT.SF.hOct34co.hKlf4co.hSox2co.hmyc.idTomato.pre.FRT (Supplementary CTAT Table). After two days cells were transferred to vitronectin-coated (ThermoFisher) vessels and cultured in Essential-6 medium (ThermoFisher) with 10ng/ml FGF. When nascent iPSC colonies appeared, medium was switched to Essential-8 medium (ThermoFisher) for colony expansion. After two weeks, iPSC colonies were isolated and cultured for >6 passages.

Embryoid body formation assay

Embryoid bodies (EB) were generated by detaching iPSC colonies with 0.5mM EDTA in PBS. Aggregates were transferred to Ultra-Low attachment flasks (Corning) and cultured in Essential-8 overnight. EB's were cultured in KnockOut™ Serum-Replacement-medium (ThermoFisher) for 10d. Then, EB were transferred to hESC-qualified matrigel (BD/Biosciences)-coated coverslips and cultured for another 4d in KnockOut™SR. EB were fixed in 4% paraformaldehyde and immunohistochemically analyzed.

Stem cell culture

All human pluripotent stem cell lines (Supplementary CTAT Table) were maintained on Vitronectin in Essential-8. Cells were passaged every 4-5d with 1% RevitaCell Supplement added overnight on the day of passage.

Hepatocyte differentiation

50,000 iPSC were plated as single cells in a vitronectin-coated (ThermoFisher) well and cultured in Essential-8 with RevitaCell supplement. Next day, cells were differentiated to definitive endoderm using the PSC Definitive-Endoderm-Induction Kit (ThermoFisher). After 2d, RPMI1640 (ThermoFisher) containing 20ng/ml BMP4, 10ng/ml FGF2, 0.5% DMSO (Sigma) and B27-supplement (ThermoFisher) was added for 5d for hepatic lineage specification. The hepatic progenitor cells were then transferred to ESC-qualified Matrigel-coated wells in RPMI1640 with 20ng/ml HGF, 0.5% DMSO and B27-supplement, with 1% RevitaCell supplement on the first day. Next day cells were overlaid with a ESC-qualified Matrigel and cultured for 5 more days. To promote further maturation, cells were cultured in Lonza HCM/Bulletkit medium with 20ng/ml Oncostatin-M, known to stimulate hepatocyte polarity development [27]. Medium was changed daily for all stages of differentiation. For ATP7B translocation experiments, mature hiHeps were treated with 200µM BCS (Sigma) for 8h, washed with PBS, and treated with 200µM BCS or 100µM $CuSO_4$ for 16h. For CFDA transport assay, hiHeps were incubated with 0.5µM CFDA (Sigma-Aldrich) at 37°C for 30min and analyzed with a Leica DMI 6000 fluorescent microscope. To asses LDL uptake, hiHeps were incubated with 10µg/ml DiI-LDL (Alfa-Aesar) for 4h, washed, fixed in 4% paraformaldehyde for 20min, stained with DAPI and mounted. For chemical chaperone rescue experiments, hiHeps were incubated with 5mM PBA or 5µM curcumin 48h prior to and during $CuSO_4$ treatment.

Western blotting

Cell lysates were prepared in RIPA buffer (150 mM NaCl, 1% NP-40, 0,5% sodium deoxycholate, 0.1% SDS, 50mM Tris pH 8,0) with protease inhibitors, and mixed 1:1 with sample buffer (2% SDS, 5% β-mercaptoethanol, 0.125 M Tris–HCl, pH 6.8, 40% glycerol, 0,01% bromophenolblue) and incubated at 70°C for 10 min. Proteins were resolved by SDS-PAGE and electrotransferred onto PVDF membranes. Membranes were blocked with Odyssey blocking buffer and incubated with primary antibodies (Supplementary CTAT Table). Membranes were washed, incubated with fluorescently labeled secondary antibodies, and scanned with the Odyssey. Relative quantification was performed using the Odyssey software.

Microscopy

Immunolabeling was done as described previously [28]. For antibodies see Supplementary CTAT Table. Fluorescent images were captured on a Leica DMI 6000 fluorescent microscope and a Leica SP8 DMI 6000 confocal microscope, and analyzed using ImageJ and Adobe Photoshop. Quantification of colocalization in high-resolution confocal images was done using ImarisColoc software. Thresholds were set using the ImarisColoc automatic thresholding algorithm. Electron microscopy was performed as described previously [29]. 60nm sections imaged with a Zeiss Supra55 in STEM mode at 26KV using an external scan generator (Fibics, Canada) yielding mosaics of large area scans at 2.5nm pixel resolution.

Quantitative polymerase chain reaction

RNA was collected using TRI reagent (Sigma). Total RNA was reverse transcribed in the presence of oligo(dT)12–18 (Invitrogen) and dNTPs (Invitrogen) with M-MLV reverse transcriptase (Invitrogen) according to manufacturer's instructions. Gene expression levels were measured by real-time quantitative RT-PCR with ABsolute QPCR SYBR Green Master Mix (Westburg) in a Step-One Plus RTPCR apparatus. Resulting data analyzed using the LinRegPCR method. See supplementary information and CTAT Table for primers and detailed protocol.

Results

Differentiation of pluripotent stem cells to hepatocyte-like cells

Pluripotent HUES9 cells were differentiated toward hepatocyte-like cells (hiHeps) using a protocol based on embryonic hepatic development and previous studies on hepatocyte differentiation in culture [16,24,30] (Figure 1A). Differentiation resulted in the loss of expression of pluripotency markers and progressive expression of hepatic marker proteins, including hepatocyte nuclear factor (HNF)4-alpha, alpha-fetoprotein and albumin (Figure 1B and 2B), glutamate-ammonia ligase and carbamoyl-phosphate synthetase-1, sodium-taurocholate cotransporting polypeptide (NTCP), and alpha-1-antitrypsin (AAT) (Figure 2A). Virtually all AAT-positive HiHeps were positive for HNF4a and most HNF4a-positive cells were positive for AAT (Supplemental Figure S1A). Fluorescently labeled low-density lipoprotein was endocytosed in hiHeps (Figure 2A). Electron-microscopy showed copious quantities of glycogen in the hiHeps' cytosol (Figure 2C). Cholangiocyte markers were absent from hiHeps (supplemental Figure S1B). The differentiation yield, based on the percentage of AAT- or HNF4a-expressing HiHeps, was ~50% (Supplemental Figure S1A).

Pluripotent stem cell-derived hiHeps develop apical-basolateral polarity and form branching bile canalicular networks

The canalicular multispecific organic anion transporter 1 (cMOAT1/ABCC2) revealed the presence of branching networks of canaliculi running between adjacent mature hiHeps (Figure 3A-B). Canaliculi also contained Thr567-phosphorylated (active)

ERM-family proteins including the dominant ERM-protein in hepatocytes, radixin, which is considered a structural marker of bile canaliculi [31] (Figure 3B-C).

ABCC2 was exclusively localized to the canalicular domain (Figure 3B), flanked by the tight junction-associated protein ZO-1 (Figure 3C) [32], indicating that hiHeps developed canalicular-sinusoidal polarity. Three-dimensional reconstruction supported the lateral orientation of the canaliculi (Figure 3E), a hallmark of hepatocytes in the liver [1]. Other canalicular proteins including bile salt export pump (BSEP/ABCB11) and 5'nucleotidase (NT5E) were also restricted at the canalicular domain (Figure 3F). By contrast, anoctamin-6 (ANO6) was observed at both the apical and basolateral surface domains (Figure 3F), as in vivo. The fluorescent ABCC2 substrate 5-chloromethylfluorescein (CFDA) [31] was secreted and retained in the canaliculi of living hiHeps (Figure 3F), supporting the luminal nature of the bile canaliculi. Electron-microscopy confirmed the presence bile canaliculi with microvilli and associated tight junctions (Figure 3G). Notably, all hiHeps that formed bile canaliculi expressed the AAT protein (Figure 3D, Supplemental Figure S1C), indicating that these represented well-differentiated hiHeps. Together, human pluripotent stem cell-derived hiHeps developed apical-basolateral polarity and formed bile canaliculi.

Polarized hiHeps recapitulate polarized trafficking processes

To investigate whether the polarized hiHeps recapitulated regulated polarized trafficking processes, we examined the ability of copper to trigger the redistribution of the copper transporter ATP7B from TGN to the canalicular domain [3,12,33]. During HUES9 differentiation to hiHeps ATP7B was expressed from the endoderm stage

(Figure 4A). In mature hiHeps ATP7B colocalized with the TGN marker Golgin-97 (Figure 4B) and was absent from the ABCC2-labeled canaliculi (Figure 4C,D) under copper-chelated conditions. Copper-treatment resulted in reduced ATP7B colocalization with Golgin-97 (Figure 4B) and its appearance at the ZO-1-bordered canaliculi (Figure 4C-D). ATP7B in copper-treated hiHeps also appeared at LAMP1-positive compartments (Figure 4E), which have been implicated in the trafficking of ATP7B to the bile canaliculi [12,23] although debated [34]. Fluorescence intensity boxplots covering the intracellular ATP7B compartments and the canalicular domain illustrated ATP7B translocation by the appearance of overlapping ABCC2 and ATP7B peaks in the copper-treated conditions (Figure 4F). To obtain a measure of ATP7B canalicular translocation that was representative of the population as a whole, these intensity plots were used to determine the relative ATP7B intensity at the maximum relative intensity of ABCC2 for multiple canaliculi. Resultant dotplots showed that in copper-treated hiHeps, ATP7B staining is significantly more intense at the canalicular domain for the majority of canaliculi, when compared to BCS-treated controls (Figure 4G).

Pluripotent stem cells can also be generated by reprogramming somatic cells from any individual. The differentiation of these induced pluripotent stem cells (iPSC) from healthy individual's somatic cells to hiHeps (Control-1) yielded similar results when compared to HUES9-derived hiHeps, including development of cell polarity and bile canaliculi (supplemental Figure S2A-B) and the copper-stimulated canalicular redistribution of ATP7B (Figure 5A-D).

These data show that hiHeps not only developed apical-basolateral polarity and formed bile canaliculi, but also recapitulated regulated polarized trafficking processes.

Endogenously expressed mutant ATP7B-H1069Q shows defective copper-stimulated redistribution to the bile canalicular domain

The ability of iPSC-derived hiHeps to develop apical-basolateral polarity, form bile canaliculi and recapitulate regulated polarized trafficking processes allowed us to for the first time characterize the polarized trafficking phenotype of endogenously expressed mutant ATP7B proteins. We generated urine cell-derived iPSC (supplemental Figure S3A-C) and thereof derived hiHeps of a WD patient (WD1) who presented advanced liver fibrosis at age 13 and has a compound heterozygous nonsense W779X and missense H1069Q mutation in the *ATP7B* gene. This was confirmed in the patient's iPS (supplemental Figure S4A). H1069Q is the most common *ATP7B* mutation in the Caucasian WD population and presumed to lead to folding defects and retention of the mutant protein in the endoplasmic reticulum (ER) and its degradation [35]. The also common nonsense W779X mutation causes depletion of the protein. In accordance, Western blot analysis revealed the presence of a single band at the molecular weight of ATP7B and no truncated products in the WD hiHeps (Figure 6A).

ATP7B expression was lower in WD hiHeps when compared to control hiHeps (Figure 6A,B). The protein reduction exceeded mRNA reduction (Figure 6C), supporting the previously reported increased degradation rate of ATP7B-H1069Q [23]. Importantly, WD and HUES9 showed similar differentiation yields, as determined by the percentage of AAT- and HNF4a-expressing hiHeps (Supplemental Figure S1A). Further, WD hiHeps developed apical-basal polarity and bile canaliculi, indicating that functional ATP7B is not essential for hepatocyte polarity (Figure 6F). In WD hiHeps, ATP7B-H1069Q co-distributed with the TGN marker under copper-

chelated culture conditions (Figure 6D, supplemental Figure S5A), indistinguishable from HUES9 cell-derived hiHeps (*c.f.*, Figure 4B) and iPSC-derived hiHeps of control individuals (*c.f.*, Figure 5A). Quantitative colocalization analyses revealed no difference between the extent of ATP7B or ATP7B-H1069Q colocalization with the TGN (supplemental Figure S5B). However, in striking contrast to control iPSC- and HUES9-derived hiHeps, exposure of WD hiHeps to copper failed to trigger the redistribution of ATP7B-H1069Q to the canalicular domain (Figure 6F-H, respectively). Similar results were obtained with hiHeps derived from iPSC of an unrelated WD patient (WD2) with homozygous H1069Q/H1069Q mutations. Thus, hiHeps of this patient confirmed the significant localization of the endogenous ATP7B-H1069Q mutant protein at the TGN [25] (Supplemental Figure S7A) and the failure of the mutant protein to redistribute to the canaliculi in response to copper (Supplemental Figure S6C-E). Importantly, in hiHeps of a first-degree family member of this patient (Control-2) the copper-induced redistribution of ATP7B to the bile canaliculus was unaffected (Supplemental Figure S6A,B,E), indistinguishable from the unrelated control subject (*c.f.*, Figures 4 and 5). Notably, while copper stimulated the redistribution of ATP7B-H1069Q to LAMP1-positive compartments in hiHeps of the homozygous patient (Supplemental Figure S7C), this was not observed in hiHeps of the heterozygous H1069Q/null patient (Figure 6E). These results reveal, for the first time, the trafficking phenotypes of *endogenously expressed* mutant ATP7B proteins in *polarized* hepatocytes. They demonstrate that the H1069Q mutation in ATP7B protein does not *per se* preclude the endogenous mutant protein from reaching a steady-state distribution at the TGN but, unexpectedly, causes a defect in its copper-triggered polarized redistribution to the bile canaliculi.

Curcumin and 4-phenylbutyrate do not restore copper-induced canalicular translocation of ATP7B-H1069Q

Earlier studies have demonstrated that ATP7B-H1069Q when overexpressed in cells or present in homozygous patient tissue can be retained in the ER, which precludes its trafficking to and function at the TGN and its copper-induced redistribution to the bile canaliculi. The pharmacological folding chaperones curcumin and 4-phenylbutyrate have been reported to improve the folding, stability and trafficking of ER-retained ATP7B-H1069Q to the TGN [36]. Whether curcumin and 4-phenylbutyrate can also restore the redistribution of TGN-resident ATP7B-H1069Q to bile canaliculi in response to high copper levels has not been experimentally addressed [36]. In curcumin-treated WD hiHeps, ATP7B-H1069Q maintained its predominant TGN localization and no copper-triggered redistribution to the canaliculi was observed (Figure 7A-B). Comparable results were obtained with 4-phenylbutyrate (Figure 7A-B). Western blot analysis revealed that curcumin treatment of WD hiHeps expressing the endogenous mutant ATP7B-H1069Q protein led to a 1.5-fold increase in the expression of ATP7B-H1069Q (Figure 7C), which is commonly interpreted to reflect improved stability of the mutant protein [22,36]. Our results suggest that curcumin and 4-phenylbutyrate may not be suitable to restore ATP7B-H1069Q trafficking in all patients and demonstrate the importance of investigating the usefulness of therapeutic compounds in the context of patient-specific, autologous ATP7B mutant proteins.

AP1S1 mutations do not preclude copper-induced canalicular translocation of ATP7B in MEDNIK hiHeps

Copper overload has been reported in patients with MEDNIK syndrome who have no mutations in *ATP7B* but mutations in the *AP1S1* gene [37]. Whether copper overload in MEDNIK patients is due to a ATP7B localization or trafficking defect, as suggested [34,38], has not been determined. We generated iPSC lines from a MEDNIK patient (Supplementary Figure S3A-C and S4B) and differentiated these to hiHeps. Our data show that in MEDNIK hiHeps under control conditions, ATP7B predominantly localized at the TGN (Figure 8A). No redistribution of ATP7B to other cellular locations or the canalicular domain was observed under control conditions. Copper exposure caused ATP7B redistribution to LAMP1-positve vesicles (Figure 8B) and to the canalicular domain (Figure 8C-E), indistinguishable from copper-exposed control hiHeps (*c.f.*, Figure 4D-G and 5B-D). No accumulation of ATP7B was observed at other subcellular locations, which would be indicative for ATP7B missorting. Thus, the MEDNIK *AP1S1* mutation, as such, does not necessarily change the subcellular distribution of ATP7B or prevent its copper-induced redistribution to the canalicular domain.

Discussion

We report a stem cell-based model system that reiterates the (dys)functionality of endogenously expressed mutant proteins in the context of the polarized hepatocyte, their associated diseases and treatment responses. We show that pluripotent stem cells can be differentiated to hepatocyte-like cells (hiHeps) that 1) develop an in vivo-like branching canalicular network flanked by tight junctions, 2) establish a polarized distribution of bile canalicular membrane proteins at the apical surface domain, 3) secrete and retain bile canalicular efflux pump substrates in the canalicular lumen and, 4) display regulated polarized trafficking as exemplified by the copper-stimulated redistribution of ATP7B to the canalicular domain. Polarized iPSC-derived hiHeps offer a major advance over currently available hepatocyte model systems [39] as they allow the study of human patient-specific and endogenously expressed mutant proteins (homozygous or (compound) heterozygous) in easy to obtain and unlimited cultures of patient-own cells.

We have applied iPSC-derived hiHeps to investigate the phenotype of the most frequent *ATP7B* mutation, H1069Q, in the Caucasian WD population [9], of which the functional consequences for the protein remain enigmatic [4]. Contrasting previous studies in which ATP7B-H1069Q was overexpressed and found retained in the ER, our data show that endogenously expressed ATP7B-H1069Q at low copper levels localized at the TGN, indistinguishably from wild-type ATP7B. Possibly, there is a critical expression level of the mutant protein beyond which the chaperone-based protein quality control machinery, which can suppress the unfolding propensity of (mutant) proteins [40], becomes overwhelmed. This could result in the ER retention of superfluous mutant proteins. Such scenario is in line with the reported role of the chaperone protein HspB5 in the folding of ATP7B [41,42] and ability of the

pharmacological chaperones 4-phenylbutyrate and curcumin to suppress ER retention of ATP7B-H1069Q [36] in conditions where the mutant protein was overexpressed in cell lines. While the influence of the protein quality control capacity and other putative genetic modifiers [43–45] on endogenous ATP7B-H1069Q stability and trafficking deserves further studies, our work and that of Parisi and colleagues [23] clearly demonstrate that the H1069Q substitution in ATP7B *per se* does not preclude its trafficking to the TGN.

While the predominant ER retention of ATP7B-H1069Q when overexpressed in cell lines prohibited studies with regard to its copper-stimulated post-TGN and polarized trafficking behavior, our experiments with endogenously expressed ATP7B-H1069Q in polarized WD hiHeps now clearly demonstrate that the H1069Q mutation inhibited the copper-stimulated redistribution of ATP7B to the bile canalicular domain. Furthermore, treatment of the WD hiHeps with the folding chaperones curcumin or 4-phenylbutyrate, which can improve the stability and TGN residence of ATP7B-H1069Q under conditions where this mutant was trapped in the ER [36], failed to restore copper-stimulated redistribution of the endogenously expressed ATP7B-H1069Q to the bile canalicular domain.

Our results indicate that the disease mechanism in WD patients with the H1069Q mutation involves, in addition to the reduced expression of the mutant protein [25], a defect in the copper-stimulated redistribution of the non-degraded mutant protein to the canalicular domain. Importantly, as our findings suggest that curcumin and 4-phenylbutyrate are not likely to be effective therapeutics to promote canalicular translocation of ATP7B-H1069Q, this study underscores the potential of personalized preclinical *in vitro* model systems for the evaluation of drug efficacy, especially in the context of emerging WD treatment concepts [46].

In addition to mutations in *ATP7B* itself, mutations in genes that control ATP7B trafficking may also give rise to liver copper overload. We previously demonstrated that MEDNIK syndrome patients showed copper metabolism perturbations and hepatopathy, and MEDNIK fibroblasts showed aberrant intracellular trafficking of Menkes protein ATP7A [10]. The MEDNIK disease-causing gene *AP1S1* encodes the sigma-1 subunit of an adaptor protein complex that mediates the sorting of membrane proteins with a cytoplasmic (D/E)XXXL[L/I] signal. Like ATP7A, ATP7B contains such a signal [47] which has led to suggest that the observed copper overload in MEDNIK patients results from defective ATP7B trafficking to the bile canaliculi [34,38]. We now demonstrate that hiHeps that endogenously express the disease-causing mutations in the *AP1S1* gene do not show defects in the copper-stimulated redistribution of ATP7B to the canalicular domain in MEDNIK HiHeps. This suggests that the copper metabolism perturbation and hepatopathy in this particular MEDNIK patient may not be caused by defective ATP7B trafficking in hepatocytes.

In conclusion, investigating patient-derived polarized hiHeps that endogenously express disease-causing mutant genes and proteins revealed unexpected and new trafficking phenotypes of the ATP7B protein, as a function of mutations in *AP1S1* and as a function of the H1069Q mutation in *ATP7B*. The results demonstrate the importance of investigating the (dys)functionality of endogenously expressed mutant proteins and their response to novel therapeutic strategies in patient-own cells in which the disease-causing mutant gene is endogenously expressed. The polarity and bile canaliculi-forming capacity of iPSC-derived hiHeps, as reported in this study, is an important step forward for the study of severe and incurable inherited liver diseases in which hepatocyte polarity plays an important role.

References

[1] Treyer A, Müsch A. Hepatocyte polarity. Compr Physiol 2013;3:243–87. doi:10.1002/cphy.c120009.

[2] Gissen P, Arias IM. Structural and functional hepatocyte polarity and liver disease. J Hepatol 2015;63:1023–37. doi:10.1016/j.jhep.2015.06.015.

[3] Roelofsen H, Wolters H, Van Luyn MJ, Miura N, Kuipers F, Vonk RJ. Copper-induced apical trafficking of ATP7B in polarized hepatoma cells provides a mechanism for biliary copper excretion. Gastroenterology 2000;119:782–93.

[4] Bartee MY, Lutsenko S. Hepatic copper-transporting ATPase ATP7B: function and inactivation at the molecular and cellular level. Biometals Int J Role Met Ions Biol Biochem Med 2007;20:627–37. doi:10.1007/s10534-006-9074-3.

[5] Bull PC, Thomas GR, Rommens JM, Forbes JR, Cox DW. The Wilson disease gene is a putative copper transporting P-type ATPase similar to the Menkes gene. Nat Genet 1993;5:327–37. doi:10.1038/ng1293-327.

[6] Ferenci P. Pathophysiology and clinical features of Wilson disease. Metab Brain Dis 2004;19:229–39.

[7] Thomas GR, Forbes JR, Roberts EA, Walshe JM, Cox DW. The Wilson disease gene: spectrum of mutations and their consequences. Nat Genet 1995;9:210–7. doi:10.1038/ng0295-210.

[8] Ferenci P, Roberts EA. Defining Wilson disease phenotypes: from the patient to the bench and back again. Gastroenterology 2012;142:692–6. doi:10.1053/j.gastro.2012.02.035.

[9] Ferenci P. Regional distribution of mutations of the ATP7B gene in patients with Wilson disease: impact on genetic testing. Hum Genet 2006;120:151–9. doi:10.1007/s00439-006-0202-5.

[10] Martinelli D, Travaglini L, Drouin CA, Ceballos-Picot I, Rizza T, Bertini E, et al. MEDNIK syndrome: a novel defect of copper metabolism treatable by zinc acetate therapy. Brain J Neurol 2013;136:872–81. doi:10.1093/brain/awt012.

[11] Gupta A, Bhattacharjee A, Dmitriev OY, Nokhrin S, Braiterman L, Hubbard AL, et al. Cellular copper levels determine the phenotype of the Arg875 variant of ATP7B/Wilson disease protein. Proc Natl Acad Sci U S A 2011;108:5390–5. doi:10.1073/pnas.1014959108.

[12] Polishchuk EV, Concilli M, Iacobacci S, Chesi G, Pastore N, Piccolo P, et al. Wilson disease protein ATP7B utilizes lysosomal exocytosis to maintain copper homeostasis. Dev Cell 2014;29:686–700. doi:10.1016/j.devcel.2014.04.033.

[13] Braiterman LT, Murthy A, Jayakanthan S, Nyasae L, Tzeng E, Gromadzka G, et al. Distinct phenotype of a Wilson disease mutation reveals a novel trafficking determinant in the copper transporter ATP7B. Proc Natl Acad Sci U S A 2014;111:E1364-1373. doi:10.1073/pnas.1314161111.

[14] Huster D, Kühne A, Bhattacharjee A, Raines L, Jantsch V, Noe J, et al. Diverse functional properties of Wilson disease ATP7B variants. Gastroenterology 2012;142:947-956.e5. doi:10.1053/j.gastro.2011.12.048.

[15] Moriya H. Quantitative nature of overexpression experiments. Mol Biol Cell 2015;26:3932–9. doi:10.1091/mbc.E15-07-0512.

[16] Imagawa K, Takayama K, Isoyama S, Tanikawa K, Shinkai M, Harada K, et al. Generation of a bile salt export pump deficiency model using patient-specific induced pluripotent stem cell-derived hepatocyte-like cells. Sci Rep 2017;7:41806. doi:10.1038/srep41806.

[17] Omer L, Hudson EA, Zheng S, Hoying JB, Shan Y, Boyd NL. CRISPR Correction of a Homozygous Low-Density Lipoprotein Receptor Mutation in Familial Hypercholesterolemia Induced Pluripotent Stem Cells. Hepatol Commun 2017;1:886–98. doi:10.1002/hep4.1110.
[18] Zanoni P, Khetarpal SA, Larach DB, Hancock-Cerutti WF, Millar JS, Cuchel M, et al. Rare variant in scavenger receptor BI raises HDL cholesterol and increases risk of coronary heart disease. Science 2016;351:1166–71. doi:10.1126/science.aad3517.
[19] Yang J, Wang Y, Zhou T, Wong L-Y, Tian X-Y, Hong X, et al. Generation of Human Liver Chimeric Mice with Hepatocytes from Familial Hypercholesterolemia Induced Pluripotent Stem Cells. Stem Cell Rep 2017;8:605–18. doi:10.1016/j.stemcr.2017.01.027.
[20] Tafaleng EN, Chakraborty S, Han B, Hale P, Wu W, Soto-Gutierrez A, et al. Induced pluripotent stem cells model personalized variations in liver disease resulting from α1-antitrypsin deficiency. Hepatol Baltim Md 2015;62:147–57. doi:10.1002/hep.27753.
[21] Cayo MA, Cai J, DeLaForest A, Noto FK, Nagaoka M, Clark BS, et al. JD induced pluripotent stem cell-derived hepatocytes faithfully recapitulate the pathophysiology of familial hypercholesterolemia. Hepatol Baltim Md 2012;56:2163–71. doi:10.1002/hep.25871.
[22] Zhang S, Chen S, Li W, Guo X, Zhao P, Xu J, et al. Rescue of ATP7B function in hepatocyte-like cells from Wilson's disease induced pluripotent stem cells using gene therapy or the chaperone drug curcumin. Hum Mol Genet 2011;20:3176–87. doi:10.1093/hmg/ddr223.
[23] Parisi S, Polishchuk EV, Allocca S, Ciano M, Musto A, Gallo M, et al. Characterization of the most frequent ATP7B mutation causing Wilson disease in hepatocytes from patient induced pluripotent stem cells. Sci Rep 2018;8:6247. doi:10.1038/s41598-018-24717-0.
[24] Si-Tayeb K, Idriss S, Champon B, Caillaud A, Pichelin M, Arnaud L, et al. Urine-sample-derived human induced pluripotent stem cells as a model to study PCSK9-mediated autosomal dominant hypercholesterolemia. Dis Model Mech 2016;9:81–90. doi:10.1242/dmm.022277.
[25] Parisi S, Polishchuk EV, Allocca S, Ciano M, Musto A, Gallo M, et al. Characterization of the most frequent ATP7B mutation causing Wilson disease in hepatocytes from patient induced pluripotent stem cells. Sci Rep 2018;8:6247. doi:10.1038/s41598-018-24717-0.
[26] Zhou T, Benda C, Dunzinger S, Huang Y, Ho JC, Yang J, et al. Generation of human induced pluripotent stem cells from urine samples. Nat Protoc 2012;7:2080–9. doi:10.1038/nprot.2012.115.
[27] van der Wouden JM, van IJzendoorn SCD, Hoekstra D. Oncostatin M regulates membrane traffic and stimulates bile canalicular membrane biogenesis in HepG2 cells. EMBO J 2002;21:6409–18.
[28] Van IJzendoorn SCD, Théard D, Van Der Wouden JM, Visser W, Wojtal KA, Hoekstra D. Oncostatin M-stimulated apical plasma membrane biogenesis requires p27(Kip1)-regulated cell cycle dynamics. Mol Biol Cell 2004;15:4105–14. doi:10.1091/mbc.e04-03-0201.
[29] Szperl AM, Golachowska MR, Bruinenberg M, Prekeris R, Thunnissen A-MWH, Karrenbeld A, et al. Functional characterization of mutations in the myosin Vb gene associated with microvillus inclusion disease. J Pediatr Gastroenterol Nutr 2011;52:307–13. doi:10.1097/MPG.0b013e3181eea177.
[30] Griscelli F, Ezanno H, Soubeyrand M, Feraud O, Oudrhiri N, Bonnefond A, et al. Generation of an induced pluripotent stem cell (iPSC) line from a patient with maturity-

onset diabetes of the young type 3 (MODY3) carrying a hepatocyte nuclear factor 1-alpha (HNF1A) mutation. Stem Cell Res 2018;29:56–9. doi:10.1016/j.scr.2018.02.017.
[31] Wang W, Soroka CJ, Mennone A, Rahner C, Harry K, Pypaert M, et al. Radixin is required to maintain apical canalicular membrane structure and function in rat hepatocytes. Gastroenterology 2006;131:878–84. doi:10.1053/j.gastro.2006.06.013.
[32] Anderson JM, Stevenson BR, Jesaitis LA, Goodenough DA, Mooseker MS. Characterization of ZO-1, a protein component of the tight junction from mouse liver and Madin-Darby canine kidney cells. J Cell Biol 1988;106:1141–9.
[33] Schaefer M, Roelofsen H, Wolters H, Hofmann WJ, Müller M, Kuipers F, et al. Localization of the Wilson's disease protein in human liver. Gastroenterology 1999;117:1380–5.
[34] Lalioti V, Peiró R, Pérez-Berlanga M, Tsuchiya Y, Muñoz A, Villalba T, et al. Basolateral sorting and transcytosis define the Cu+-regulated translocation of ATP7B to the bile canaliculus. J Cell Sci 2016;129:2190–201. doi:10.1242/jcs.184663.
[35] Dmitriev OY, Bhattacharjee A, Nokhrin S, Uhlemann E-ME, Lutsenko S. Difference in stability of the N-domain underlies distinct intracellular properties of the E1064A and H1069Q mutants of copper-transporting ATPase ATP7B. J Biol Chem 2011;286:16355–62. doi:10.1074/jbc.M110.198101.
[36] van den Berghe PVE, Stapelbroek JM, Krieger E, de Bie P, van de Graaf SFJ, de Groot REA, et al. Reduced expression of ATP7B affected by Wilson disease-causing mutations is rescued by pharmacological folding chaperones 4-phenylbutyrate and curcumin. Hepatol Baltim Md 2009;50:1783–95. doi:10.1002/hep.23209.
[37] Montpetit A, Côté S, Brustein E, Drouin CA, Lapointe L, Boudreau M, et al. Disruption of AP1S1, causing a novel neurocutaneous syndrome, perturbs development of the skin and spinal cord. PLoS Genet 2008;4:e1000296. doi:10.1371/journal.pgen.1000296.
[38] Martinelli D, Dionisi-Vici C. AP1S1 defect causing MEDNIK syndrome: a new adaptinopathy associated with defective copper metabolism. Ann N Y Acad Sci 2014;1314:55–63. doi:10.1111/nyas.12426.
[39] Decaens C, Durand M, Grosse B, Cassio D. Which in vitro models could be best used to study hepatocyte polarity? Biol Cell 2008;100:387–98. doi:10.1042/BC20070127.
[40] Bagdany M, Veit G, Fukuda R, Avramescu RG, Okiyoneda T, Baaklini I, et al. Chaperones rescue the energetic landscape of mutant CFTR at single molecule and in cell. Nat Commun 2017;8:398. doi:10.1038/s41467-017-00444-4.
[41] D'Agostino M, Lemma V, Chesi G, Stornaiuolo M, Cannata Serio M, D'Ambrosio C, et al. The cytosolic chaperone α-crystallin B rescues folding and compartmentalization of misfolded multispan transmembrane proteins. J Cell Sci 2013;126:4160–72. doi:10.1242/jcs.125443.
[42] Allocca S, Ciano M, Ciardulli MC, D'Ambrosio C, Scaloni A, Sarnataro D, et al. An αB-Crystallin Peptide Rescues Compartmentalization and Trafficking Response to Cu Overload of ATP7B-H1069Q, the Most Frequent Cause of Wilson Disease in the Caucasian Population. Int J Mol Sci 2018;19. doi:10.3390/ijms19071892.
[43] Medici V, Weiss K-H. Genetic and environmental modifiers of Wilson disease. Handb Clin Neurol 2017;142:35–41. doi:10.1016/B978-0-444-63625-6.00004-5.
[44] Weiss KH, Runz H, Noe B, Gotthardt DN, Merle U, Ferenci P, et al. Genetic analysis of BIRC4/XIAP as a putative modifier gene of Wilson disease. J Inherit Metab Dis 2010;33 Suppl 3:S233-240. doi:10.1007/s10545-010-9123-5.
[45] Ferenci P. Polymorphism of methylenetetrahydrofolate reductase as disease modifier - a déjà-vu in Wilson disease? J Hepatol 2011;55:753–5. doi:10.1016/j.jhep.2011.02.025.
[46] Rupp C, Stremmel W, Weiss K-H. Novel perspectives on Wilson disease treatment. Handb Clin Neurol 2017;142:225–30. doi:10.1016/B978-0-444-63625-6.00019-7.

[47] Lalioti V, Hernandez-Tiedra S, Sandoval IV. DKWSLLL, a versatile DXXXLL-type signal with distinct roles in the Cu(+)-regulated trafficking of ATP7B. Traffic Cph Den 2014;15:839–60. doi:10.1111/tra.12176.

Figure Legends

Figure 1. Differentiating HUES9 cells progressively acquire hepatic markers during directed differentiation to hiHeps

(A) Schematic overview of differentiation protocol with phase-contrast images of cells at each differentiation step. (B) Fluorescence microscopy images of different hiHep differentiation stage markers. Scale: 10µM.

Figure 2. Mature hiHeps express key hepatic markers and show capability of glycogen storage and LDL internalization

(A) Fluorescence microscopy images of glutamine ligase (GLUL), Carbamoyl-phosphate synthase 1 (CPS1), NTCP, AAT and internalized DiI-LDL. Scale bar of NTCP and AAT stainings: 10µM. (B) Western blot analysis of undifferentiated HUES9 (S0) and hiHeps (S4) showing expression of pluripotency and hepatocyte markers. (C) Electron microscopy show the presence of glycogen in hiHeps. Yellow box and arrow (left image) indicate magnified area depicting cytosolic glycogen (right image).

Figure 3. HiHeps form branching bile canalicular networks

(A) Fluorescence microscopy images of ABCC2 at subsequent differentiation stages. Scale bar: 10µM. (B-E) Fluorescence microscopy images of ABCC2, radixin, ERM proteins and ZO-1 at bile canaliculi. Co-staining of ABCC2 and AAT demonstrate maturity of polarized hiHeps (Figure 3D). Orthogonal views of 3D imaged bile canaliculi reveal the lateral orientation of the canaliculi (Figure 3E, right side, top). Schematic orthogonal views illustrate the formation of hepatic polarity (Figure 3E,

right side, middle and bottom). Dashed line represents the author's interpretation of a possible cell membrane arrangement not based on staining data. Dashed yellow line indicates orthogonal section plane. TJ: tight junction. BC: bile canaliculus. Scale bars: 10 µM (F) Fluorescence microscopy images of ANO6, BSEP and 5'Nucleotidase (NT5E) at the BC in hiHeps. In addition, hiHeps transported the fluorescent ABCC2 substrate CFDA into BC lumens. White arrows: apical ANO6, yellow arrowheads: basolateral ANO6. Scale bars: 10µM (G) Electron microscopy showing small lumens with villi (white arrows) between hiHeps, which display microvilli formation at the apical surface enclosed by tight junctions (yellow arrowheads) and desmosomes (red arrowhead).

Figure 4. Polarized HUES9-derived hiHeps recapitulate copper-stimulated ATP7B translocation

(A) Fluorescence microscopy images of ATP7B in the subsequent differentiation stages. (B) Fluorescence microscopy images of ATP7B and Golgin97 (B), ATP7B and ZO-1 (C), ATP7B and ABCC2 (D), and ATP7B and LAMP1 (E) in mature BCS-treated (white arrows) and $CuSO_4$-treated (white arrows) HUES9-derived hiHeps in BCS, white arrows). Scale bars: 10µM. Yellow arrowhead indicates ATP7B at the BC. Scale bars: 10µM (F) Fluorescence intensity profile plots along the polarization axis (areas indicated by yellow brackets in Figure 3D, yellow arrows indicate plot direction) showing overlapping ABCC2 and ATP7B intensity peaks in copper treated hiHeps but not in control. (G) Graph depicting the percentage values of ATP7B intensity at which the ABCC2 intensity is at its maximum (e.g. 3.8% for BCS condition and 84.7% for CuSO4 condition in figure 4F) for multiple BC. Error bars indicate

standard error of the mean. Asterisks indicate statistical significance (P <0.001) based on Mann–Whitney U test.

Figure 5. HiHeps derived from healthy control iPSC recapitulate copper-stimulated ATP7B translocation

(A-B) Fluorescence microscopy images of ATP7B and Golgin-97 (A) and ATP7B and ABCC2 (B) in BCS-treated and copper-treated control iPSC derived hiHeps (Control-1). Scale bars: 10µM. (C) Fluorescence intensity profile plots along the polarization axis (areas indicated by yellow brackets in Figure 3D, yellow arrows indicate plot direction) showing clear overlap of ABCC2 and ATP7B intensity peaks in copper treated hiHeps, but not in control. (D) Graph depicts the percentage values of ATP7B intensity at which the ABCC2 intensity is at its maximum (12.3% for BCS condition and 85.7% for CuSO4 condition in figure 5B) for multiple BCs. Error bars indicate SEM. Asterisks: significance (p<0.001) based on Mann–Whitney U-test.

Figure 6. Mutant ATP7B-H1069Q localizes to the TGN but does not translocate to the canalicular domain upon copper exposure

(A) Blot of WD1 H1069Q/W779X hiHeps showing expression of ATP7B-H1069Q of wildtype length. No ATP7B-W779X expression was observed. Note that the ATP7B antibody epitope is located before the W779 and an 80kDA band is expected for the truncated product. (B) Quantification of three independent WD1 hiHeps ATP7B blots relative to Hues9. Significance testing of WD1 column was done to a hypothetical value of 1. (C) Relative expression of ATP7B mRNA in Hues9 and WD1 hiHeps. (D-F) Fluorescence microscopy images of ATP7B-H1069Q and Golgin-97 (D), ATP7B-

H1069Q and LAMP1 (E), ad ATP7B-H1069Q and ABCC2 (F) in BCS- and copper-treated WD iPSC derived hiHeps (BCS and CuSO4, white arrows). Scale bars: 10µM. (G) Fluorescence intensity profile plots along the polarization axis (areas indicated by yellow brackets, yellow arrows indicate plot direction) showing no overlap of ABCC2 and ATP7B intensity peaks in copper-treated hiHeps. (H) Graph depicting the percentage values of ATP7B intensity at which the ABCC2 intensity is at its maximum (e.g. 24.1% for BCS condition and 3.6% for CuSO4 condition in figure 6D) for multiple WD H1069Q/W779X hiHep BC's. Error bars indicate standard error of the mean. No significant difference was observed between means of BCS and CuSO4 conditions (p= 0.445 based on Mann–Whitney U-test).

Figure 7. Curcumin and 4-phenylbutyrate do not restore copper-induced canalicular translocation of ATP7B-H1069Q

(A) Fluorescence microscopy images of ATP7B/H1069Q and ABCC2 in curcumin- or 4-PBA-pretreated and copper-treated WD hiHeps and hereof derived fluorescence intensity plots (plot areas indicated by yellow brackets, yellow arrows indicate plot direction). (B) Graph depicting the percentage values of ATP7B intensity at which the ABCC2 intensity is at its maximum for multiple BC in each condition. Note: HUES9 data points are the same as depicted in figure 4G and data points from BCS and $CuSO_4$ conditions are the same as depicted in figure 6F. No significant difference was observed upon PBA treatment compared to $CuSO_4$ alone (p=0.126)Mann–Whitney U-test), or upon curcumin treatment compared to $CuSO_4$ alone (p=0.227 (Mann–Whitney U-test). (C) Blot showing ATP7B-H1069Q expression in curcumin-treated hiHeps and graph depicting quantification of ATP7B-H1069Q signal relative to actin.

Figure 8. Copper stimulates ATP7B redistribution to the canalicular domain In MEDNIK syndrome hiHeps

(A-C) Fluorescence microscopy images of ATP7B and Golgin-97 (A), ATP7B and LAMP1 (B), ATP7B and ABCC2 (C) in BCS-treated and copper-treated MEDNIK hiHeps. Scale bars: 10µM. (D) Fluorescence intensity profile plots along the polarization axis (areas indicated by yellow brackets, yellow arrows indicate plot direction) showing overlapping ABCC2 and ATP7B intensity peaks in copper treated hiHeps, but not in control. (E) Graph depicting the percentage values of ATP7B intensity at which the ABCC2 intensity is at its maximum for multiple BCs. Error bars represent SEM. Asterisks: significance ($p<0.001$) (Mann–Whitney U-test).

Highlights

- Functional cell polarity can be achieved in patient pluripotent stem cell-derived hepatocytes, which allows the study of autologous mutant proteins in biliary processes.
- The most frequent Wilson disease-causing ATP7B-H1069Q mutation prevents its copper-induced polarized redistribution to the bile canalicular domain.
- MEDNIK syndrome-causing *AP1S1* gene mutations do not cause the expected defect in the copper-stimulated redistribution of ATP7B to the canalicular domain in hepatocytes

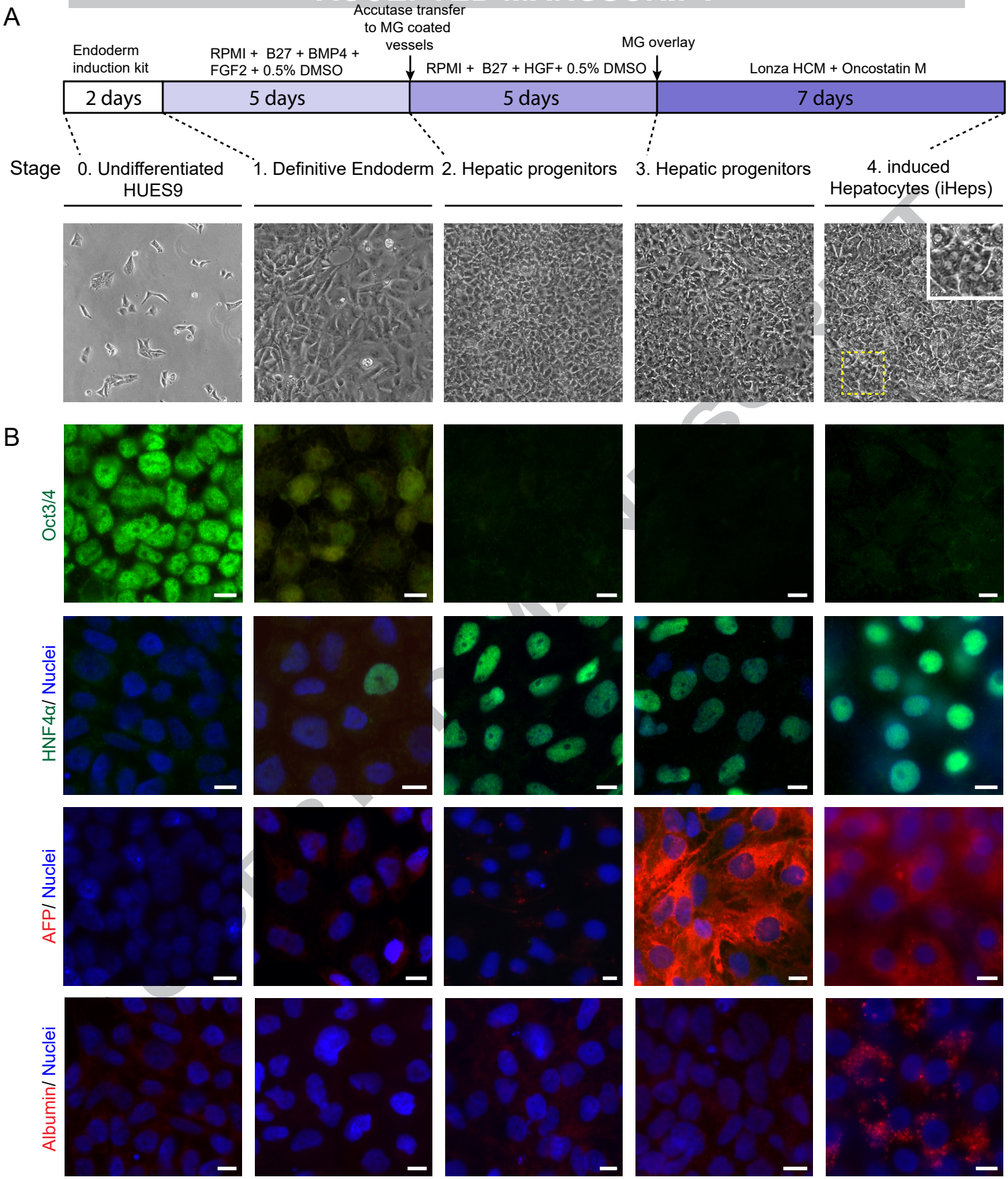

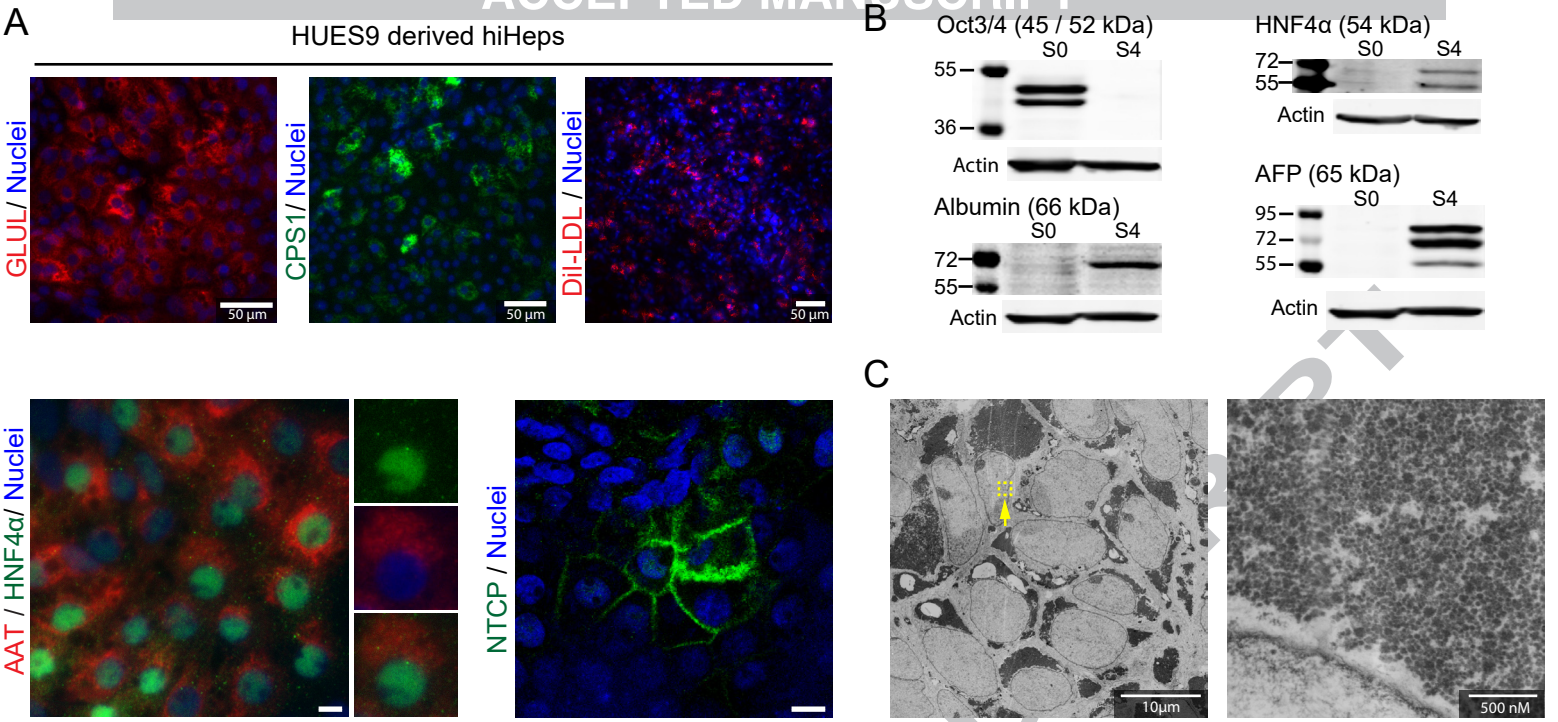

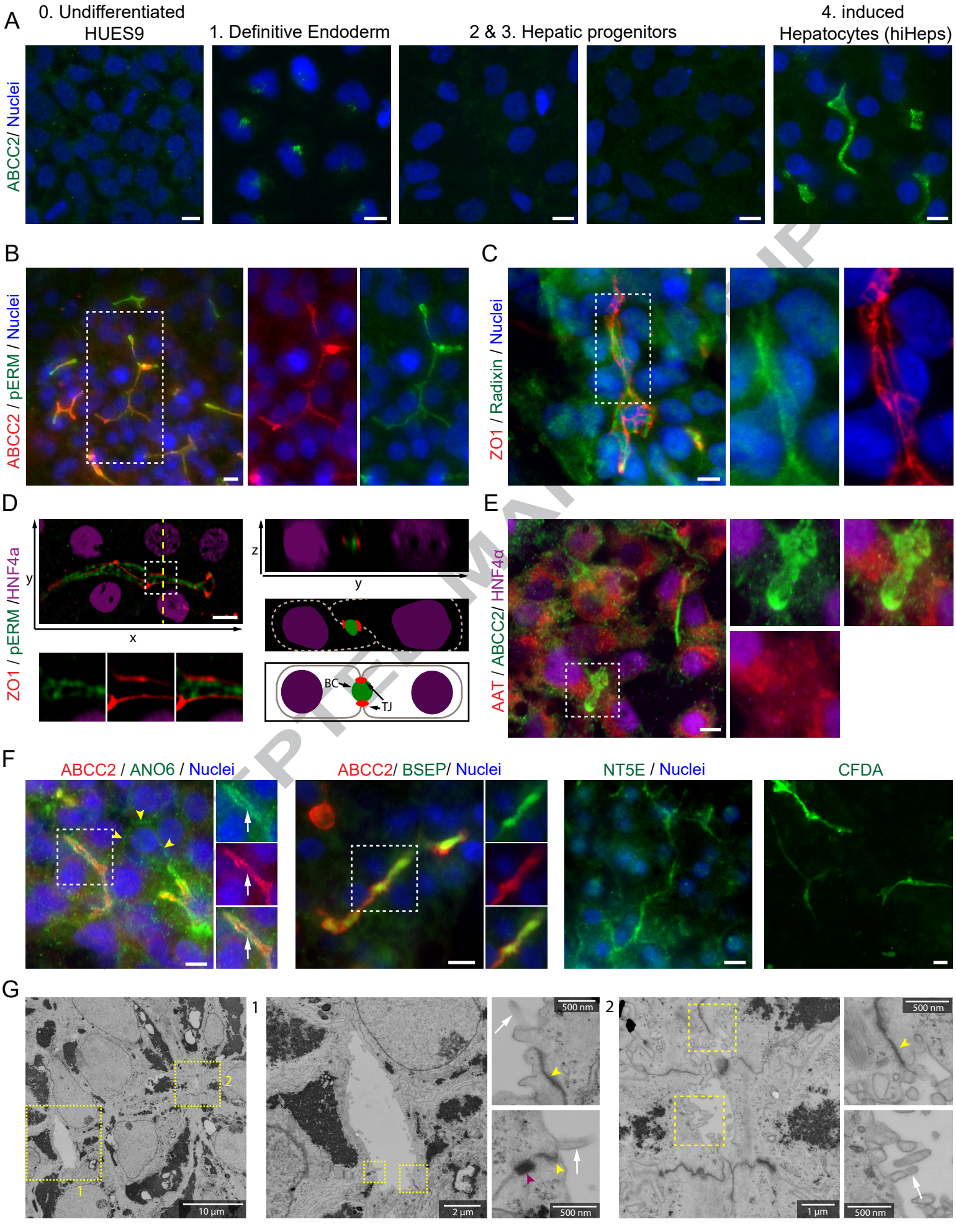

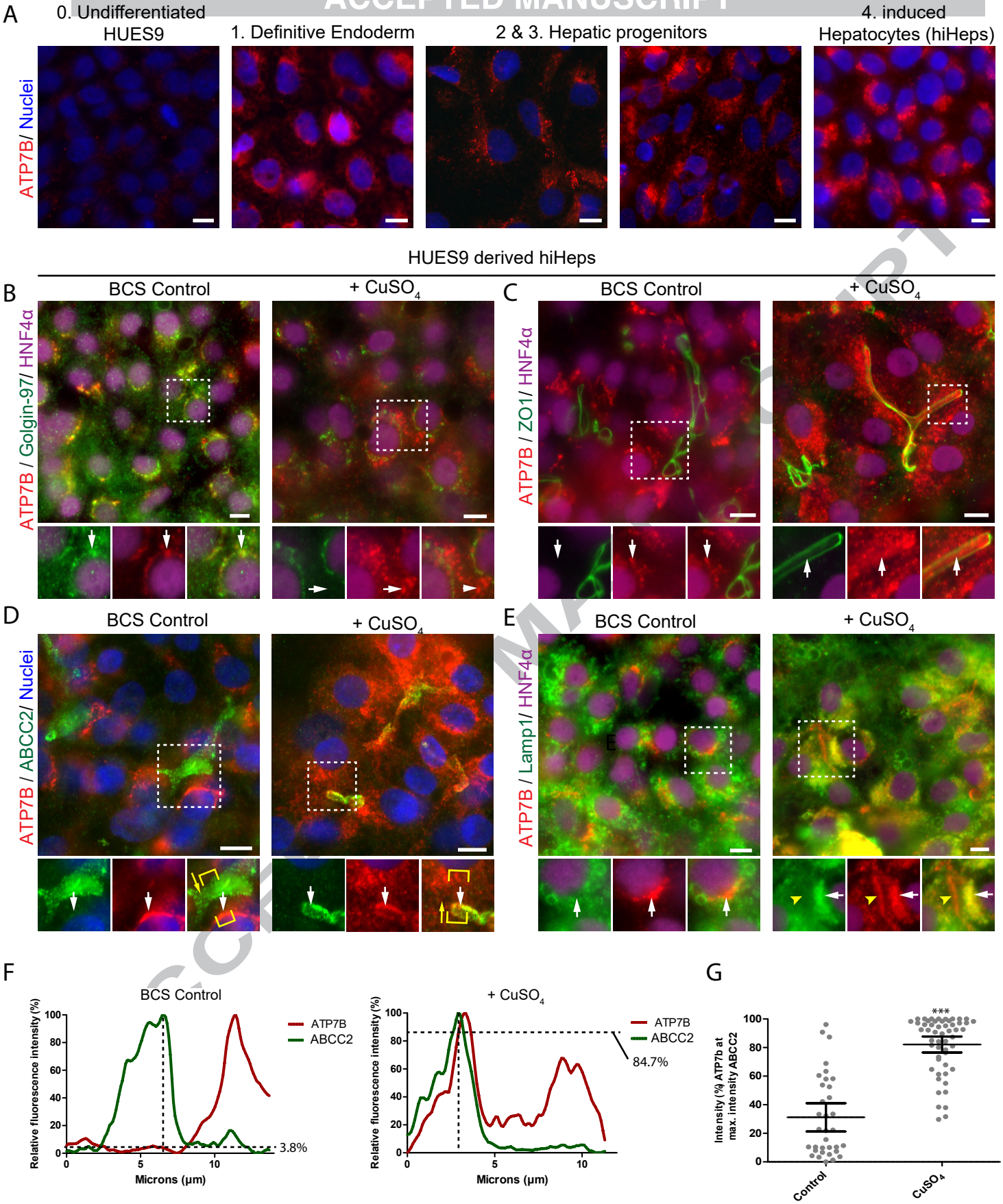

Control-1 iPSC derived iHeps

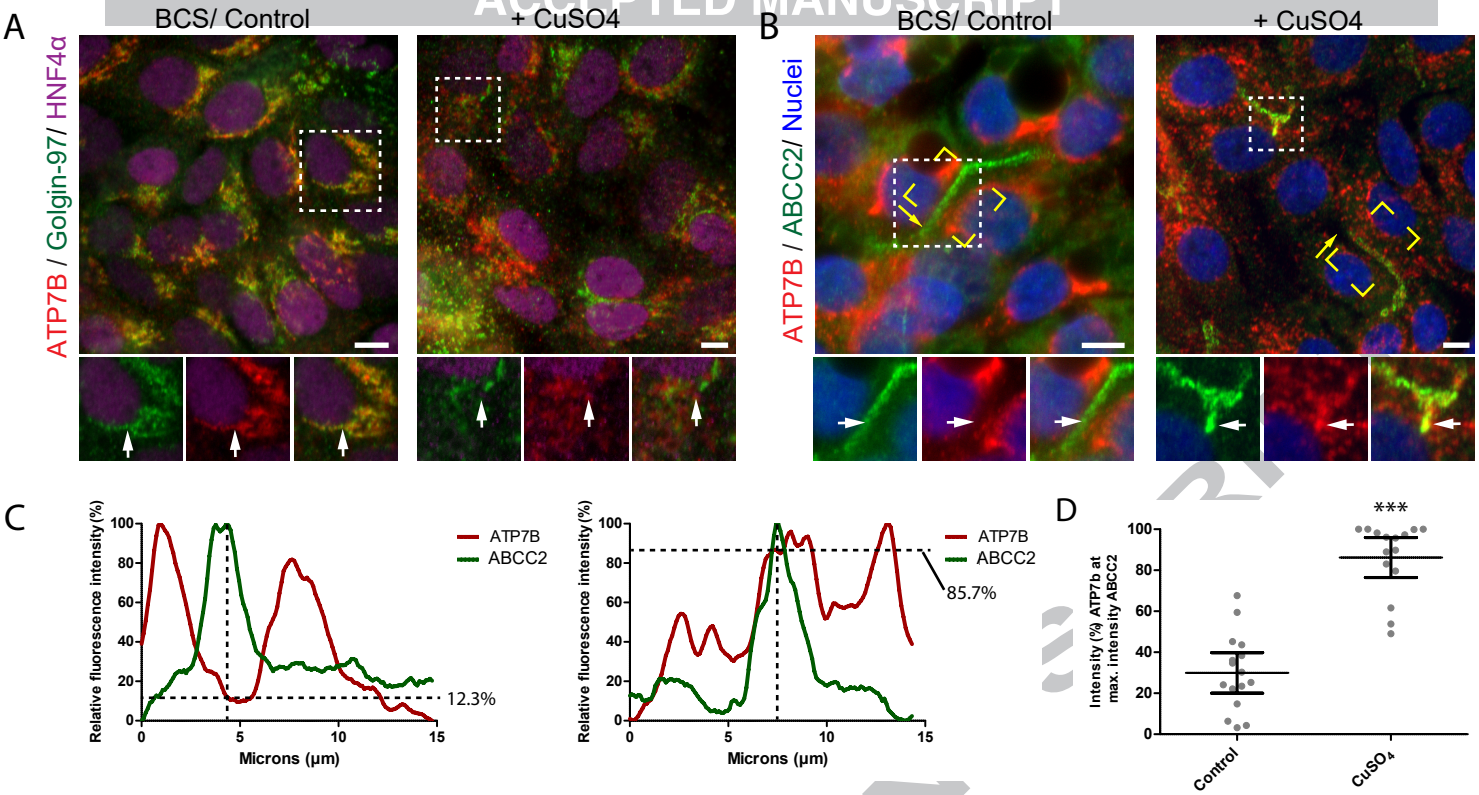

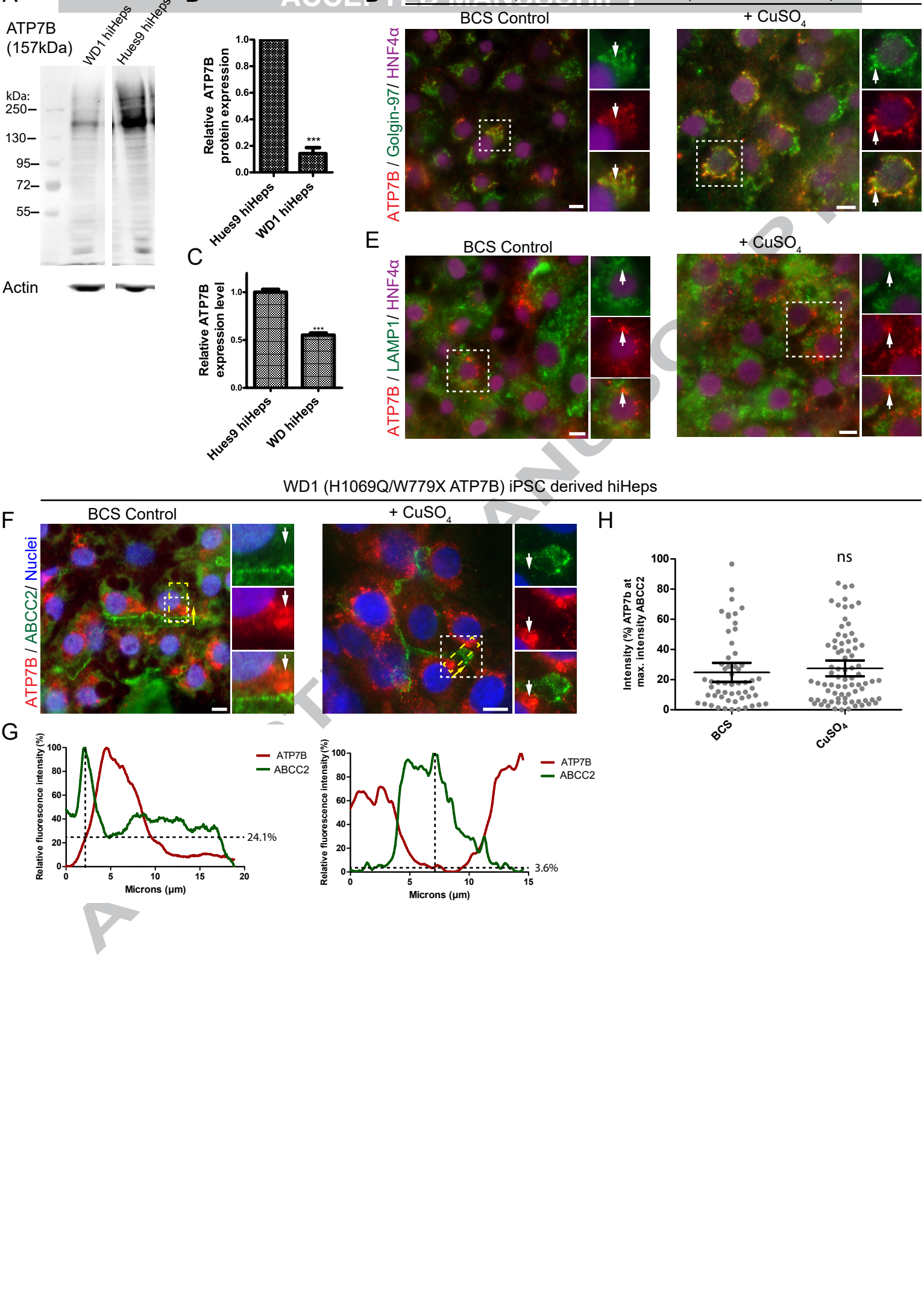

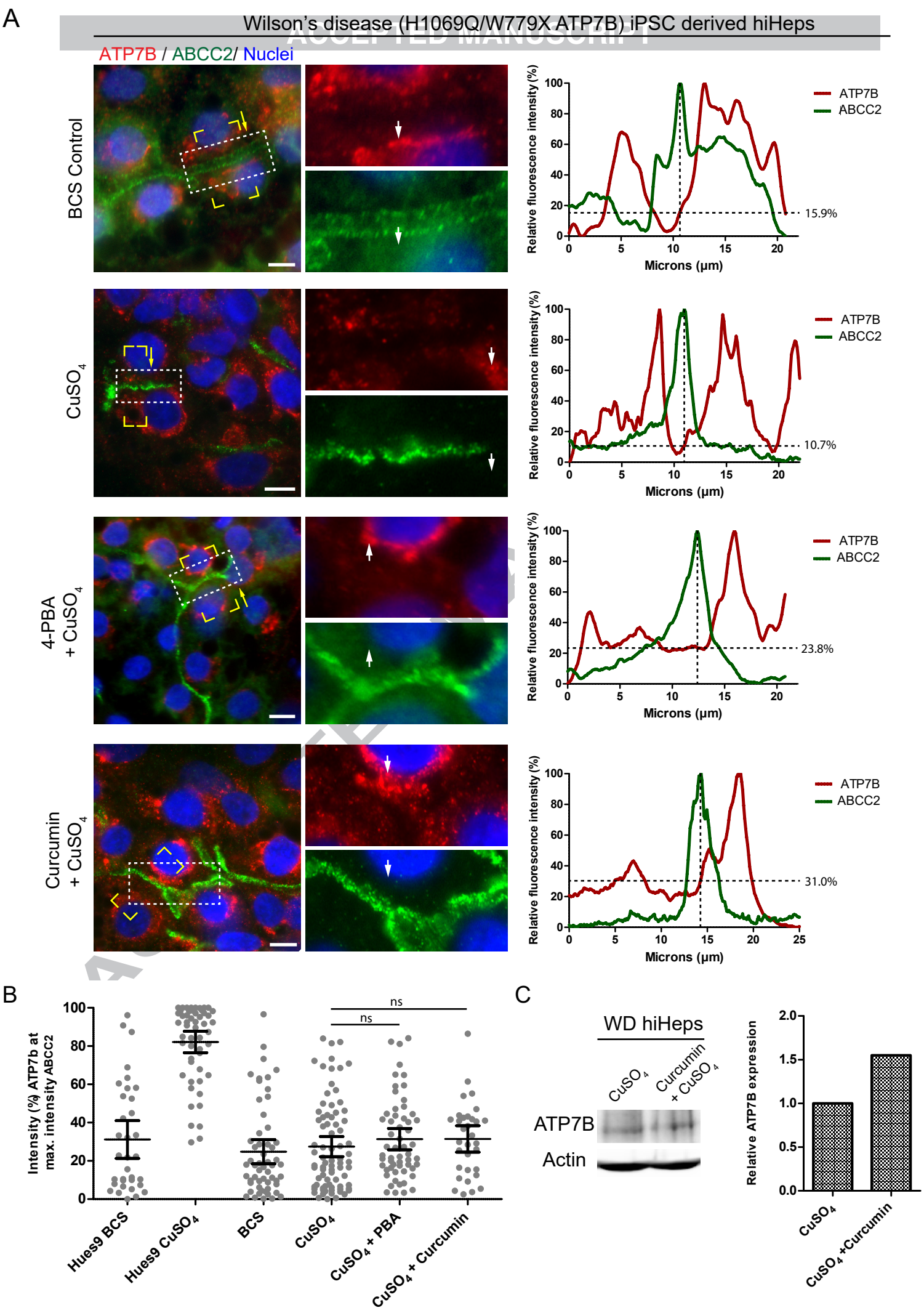

MEDNIK syndrome iPS derived hiHeps